Mechanism of Conductivity Image Contrast in MREIT: Numerical Simulation and Phantom Experiment

Y. Kim[1], T. Oh[1], A. Minhas[1], H. Kim[1], J. Seo[2], O. Kwon[3], and E. Woo[1]
[1]Biomedical Engineering, Kyung Hee University, Yongin, Gyeonggi, Korea, Republic of, [2]Computational Science and Engineering, Yonsei University, Seoul, Korea, Republic of, [3]Mathematics, Konkuk University, Seoul, Korea, Republic of

Purpose

In this paper, we explain the contrast mechanism of apparent conductivity in MREIT by performing and analyzing a series of numerical simulations and phantom imaging experiments.

Materials and Methods

Figure 1(a) shows a cross-sectional view of a homogeneous cylindrical phantom with its background conductivity of 1 S/m. It had four carbon-hydrogel electrodes attached around its side to sequentially inject currents between different electrode pairs. Figure 1(b) shows the phantom with a cylindrical anomaly at its center. The anomaly was a hollow cylinder of a transparency film (cellulose acetate, 0.3 mm thickness). We filled the phantom both inside and outside the hollow cylindrical anomaly with the same saline of 1 S/m. Figure 1(c) shows the phantom including a hollow cylinder with holes. We made four holes equally spaced around its circumference on the same *xy*-plane where four carbon-hydrogel electrodes were located. To control the contrast of apparent conductivity, we changed the diameter of the holes from 1 to 10 mm.

We built a three-dimensional model of the phantom using COMSOL (COMSOL Inc., USA). Figure 1(d) and (e) show the model of the phantom without any anomaly and its finite element mesh with 70,288 nodes and 360,086 elements whereas (f) and (g) are for the phantom including the cylindrical anomaly with four 5-mm holes. We computed *z*-components of induced magnetic flux density images denoted as B_z images on a 128×128 grid in a chosen *xy*-plane.

For imaging experiments, we located the conductivity phantom inside the bore of our 3T MRI scanner (Magnum 3, Medinus, Korea). Through two pairs of opposing electrodes, we sequentially injected currents I_1 and I_2 along two different directions. Imaging parameters were as follows: TR/TE = 1200/30 ms, FOV = 180×180 mm^2, slice thickness = 6 mm, NEX = 8, matrix size = 128×128 and number of slices = 8. We extracted B_z images from MR phase images. In addition to quantitatively analyzing and comparing both synthetic and measured B_z images, we reconstructed conductivity images using an MREIT software package called CoReHA (Conductivity Reconstructor using Harmonic Algorithms).

Results and Discussion

For all cases, we computed and measured B_z images for both horizontal and vertical injection currents. Figure 2(a) and (b) are synthetic and measured B_z images subject to horizontal injection currents, respectively, of the phantom including the hollow cylindrical anomaly with four holes of 5 mm diameter. For the horizontal injection current, only two holes along the horizontal direction are distinctly visible in the B_z images since the other two holes in the vertical direction did not pass any current. To better illustrate effects of different hole diameters on B_z images, we extracted B_z profiles of the phantom including the hollow cylindrical anomaly with four holes of 1 to 10 mm diameters. Figure 2(c) and (d) are computed and measured profiles, respectively. We can clearly see that the slope of B_z deflection or ramp changes with the hole diameter.

Figure 3 show reconstructed conductivity images of the phantom including the hollow cylinder with four holes of different diameters. We used measured B_z data sets to reconstruct the images, which can be interpreted as apparent conductivity images and also ion mobility images since ion concentrations were kept same everywhere inside the phantom. Ion mobilities inside the holes and also the internal region of the thin cylindrical wall increase as the hole diameter is enlarged. We estimated apparent conductivity values of the region inside the thin cylindrical wall including the wall itself as average pixel values within the region. Reconstructed apparent conductivity values of the cylindrical anomaly decrease as the diameter of holes gets smaller.

Conclusion

We have experimentally shown that a conductivity contrast produces deflections in magnetic flux density distributions induced by externally injected currents. Understanding the basic contrast mechanism in MREIT is crucial in properly designing experimental as well as data processing methods for high-resolution conductivity image reconstructions. Since ramp structures in magnetic flux density images provide core information on conductivity contrasts, we must preserve the structures during any MREIT data collection and processing steps. Ramp preserving must be always considered in terms of MREIT pulse sequences, denoising methods and image reconstruction algorithms.

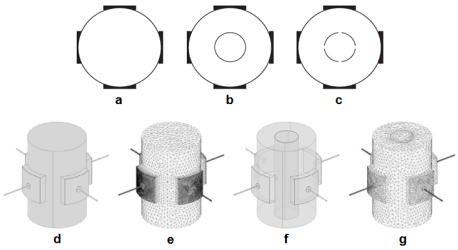

Fig. 1. Cross-sectional views of the phantom: (a) no anomaly, (b) a thin hollow cylindrical anomaly, and (c) a thin hollow cylindrical anomaly with four holes. (d) and (e) are a model and mesh of the homogeneous phantom. (f) and (g) are a model and mesh of the phantom with the cylindrical anomaly.

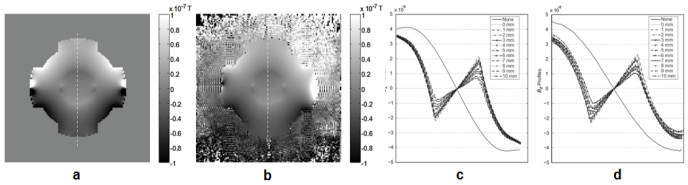

Fig. 2. B_z images of the phantom including the hollow cylindrical anomaly with holes of 5 mm diameter: (a) numerical simulation and (b) imaging experiment. Current was injected along the horizontal direction. Profiles along the dotted vertical lines are plotted: (c) numerical simulation and (d) imaging experiment.

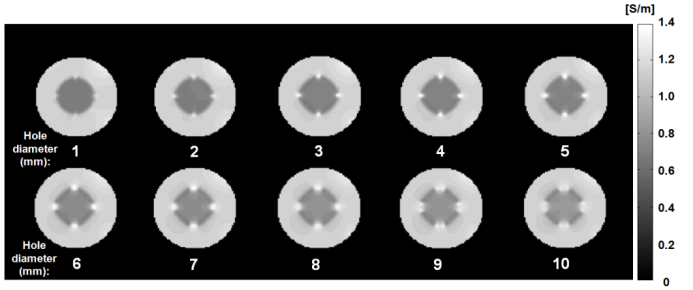

Fig. 3. Reconstructed apparent conductivity images of the phantom including the hollow cylinder with four holes of different diameters using measured B_z data sets.

References

1. Scott et al, J Magn. Reson., 97, 235-254, 1992
2. Woo et al, Physiol. Meas., 29, R1-R26, 2008
3. Kim et al, IEEE EMBS, Buenos Aires, 2010